

A VLT spectroscopic survey of RX J0152.7-1357, a forming cluster of galaxies at $z=0.837$. *

R. Demarco^{1,2}, P. Rosati¹, C. Lidman³, N. L. Homeier², E. Scannapieco⁴, N. Benítez², V. Mainieri⁵, M. Nonino⁶, M. Girardi⁷, S. A. Stanford^{8,9}, P. Tozzi⁶, S. Borgani^{10,11}, J. Silk¹², G. Squires¹³, and T. J. Broadhurst¹⁴

¹ ESO-European Southern Observatory, Karl-Schwarzschild Str. 2, D-85748 Garching b. München, Germany

² Department of Physics and Astronomy, Johns Hopkins University, 3400 N. Charles Str., Baltimore, MD 21218, USA

³ ESO-European Southern Observatory, Alonso de Cordova 3107, Casilla 19001, Santiago, Chile

⁴ Kavli Institute for Theoretical Physics, Kohn Hall, University of California, Santa Barbara, CA 93106, USA

⁵ Max-Planck-Institut für extraterrestrische Physik, Giessenbachstrasse, D-85748 Garching b. München, Germany

⁶ INAF - Osservatorio Astronomico di Trieste, via G. B. Tiepolo 11, 34131 Trieste, Italy

⁷ Dipartimento di Astronomia, Università degli Studi di Trieste, via Tiepolo 11, 34131 Trieste, Italy

⁸ Department of Physics, University of California, Davis, 1 Shields Avenue, Davis, CA 95616, USA

⁹ Participating Guest, Institute of Geophysics and Planetary Physics, Lawrence Livermore National Laboratory, USA

¹⁰ Dipartimento di Astronomia dell'Università di Trieste, via Tiepolo 11, I-34131 Trieste, Italy

¹¹ INFN - National Institute for Nuclear Physics, Trieste Universit, via Valerio 2, I-34127 Trieste, Italy

¹² Astrophysics Department, University of Oxford, Keble Road, Oxford OX1 3RH

¹³ SIRTF Science Center, California Institute of Technology, Pasadena, CA 91125, USA

¹⁴ Racah Institute of Physics, Hebrew University, Jerusalem 91904, Israel.

Abstract We present the results of an extensive spectroscopic survey of RX J0152.7-1357, one of the most massive distant clusters of galaxies known. Multi-object spectroscopy, carried out with FORS1 and FORS2 on the ESO Very Large Telescope (VLT), has allowed us to measure more than 200 redshifts in the cluster field and to confirm 102 galaxies as cluster members. The mean redshift of the cluster is $z = 0.837 \pm 0.001$ and we estimate the velocity dispersion of the overall cluster galaxy distribution to be $\sim 1600 \text{ km s}^{-1}$. The distribution of cluster members is clearly irregular, with two main clumps that follow the X-ray cluster emission mapped by Chandra. A third clump of galaxies to the east of the central structure and at the cluster redshift has also been identified. The two main clumps have velocity dispersions of ~ 919 and $\sim 737 \text{ km s}^{-1}$ respectively, and the peculiar velocity of the two clumps suggests that they will merge into a single more massive cluster. A segregation in the star formation activity of the member galaxies is observed. All star forming galaxies are located outside the high-density peaks, which are populated only by passive galaxies. A population of red galaxies (belonging to the cluster red sequence) with clear post-starburst spectral features and [OII] ($\lambda 3727$) emission lines is observed in the outskirts of the cluster. Two AGNs, which were previously confused with the diffuse X-ray emission from the intracluster medium in ROSAT and BeppoSAX observations, are found to be cluster members.

Key words. galaxies:clusters:general – techniques:spectroscopic – X-ray:galaxies:clusters – galaxies:clusters:individuals:RXJ0152.7-1357

1. Introduction

Send offprint requests to: R. Demarco (demarco@pha.jhu.edu)

* Based in part on observations carried out at the European Southern Observatory using the ESO Very Large Telescope on Cerro Paranal (ESO programs 166.A-0701, 69.A-0683 and 72.A-0759) and the ESO New Technology Telescope on Cerro La Silla (ESO program 61.A-0676).

RX J0152.7-1357 was discovered in the ROSAT Deep Cluster Survey (RDCS; Rosati et al. 1998, Della Ceca et al. 2000) as an extended double core X-ray source in the ROSAT PSPC field rp600005n00 observed in January 1992. It was independently discovered in the WARPS Survey (Ebeling et al., 2000) and reported in the Bright

SHARC survey (Romer et al. 2000). Spectroscopy of a small number of member galaxies, carried out with EFOSC1 at the ESO 3.60-m telescope at the Cerro La Silla Observatory in November 1996, spectroscopically confirmed the cluster and gave a cluster redshift of $z = 0.83$ (Della Ceca et al., 2000), placing RX J0152.7-1357 among the most distant and X-ray luminous clusters of galaxies known, akin to MS1054-03 (Donahue et al., 1998; van Dokkum et al., 1999) and RX J1716.6+6708 (Gioia et al. 1999) at $z = 0.83$ and $z=0.81$ respectively.

The ROSAT observations were used to derive a cluster X-ray luminosity¹ of $L_X = (7.4 \pm 0.7) \times 10^{44}$ erg s $^{-1}$ in the 0.5-2 keV band, and BeppoSAX observations yielded a gas temperature of $kT = 6.46^{+1.74}_{-1.19}$ keV and a metallicity of $0.53^{+0.29}_{-0.24} Z_\odot$ (Della Ceca et al. 2000). Recent observations with Chandra also show the double core structure in the intra-cluster medium (ICM) and provide some evidence of a possible merger in progress (Maughan et al. 2003; Huo et al. 2004). These two main structures, one to the north-east and the other to the south-west, are separated by ~ 1.6 (corresponding to 730 kpc at the cluster redshift) on the plane of the sky. The spectroscopic analysis of the Chandra X-ray data combined with the latest Chandra calibrations give temperatures of $6.7^{+1.2}_{-1.0}$ and $8.7^{+2.4}_{-1.8}$ keV and metallicities of $0.17^{+0.19}_{-0.16}$ and $<0.22 Z_\odot$ for the northern and southern clumps, respectively (Balestra et al., in preparation). These temperature values are consistent, within the error bars, with the BeppoSAX estimates and those reported in Ettori et al. (2004); however, the BeppoSAX metallicity (Della Ceca et al., 2000) seems to be somewhat higher than the new Chandra measurements. The X-ray temperature measurements of RX J0152.7-1357 are also consistent with Sunyaev-Zeldovich effect observations of the cluster (Joy et al. 2001).

Most of the earlier work on RX J0152.7-1357 has centered on characterizing its X-ray properties and the thermodynamical state of the hot intra-cluster gas. In this paper, we present the results of an extensive spectroscopic survey aimed at identifying a large number of galaxies belonging to the cluster. We compare our results with the X-ray information that is publicly available and with a recent weak lensing analysis of the cluster based on HST/ACS data (Jee et al. 2004), and we discuss the dynamical state of the cluster. Ground-based multi-band photometry is also used to study the distribution of cluster galaxies in colour-magnitude and colour-colour space. In forthcoming papers, we will combine the spectroscopic information presented here with HST/ACS data in a detailed study of the galaxies in RX J0152.7-1357.

2. Spectroscopic Survey

2.1. Imaging observations

We used multi-band optical and near-IR imaging observations of RX J0152.7-1357 to select targets for spectroscopy. Optical images in the B-, V-, R- and I-bands were obtained with the Low Resolution Imaging Spectrometer (LRIS; Oke et al. 1995) at the W. M. Keck Observatory. The LRIS images cover a region of $4.9' \times 6.54'$ (see Fig. 1) with a pixel scale of $0.21' \text{ pix}^{-1}$. The seeing, as measured by the FWHM of points sources, was $0.86'$ in V, $1.19'$ in B, $1.0'$ in R and $0.73'$ in I. Near-IR images in the J- and K_s-bands were obtained with SofI (Moorwood, Cuby & Lidman 1998) on the ESO NTT telescope at the Cerro La Silla Observatory. The seeing was $0.95'$ in J and $0.94'$ in K_s. The SofI images cover a region of $4.9' \times 4.9'$ (see Fig. 1) with a pixel scale of $0.29' \text{ pix}^{-1}$. The LRIS and SofI images provided the basis for the photometric catalog used to select target for spectroscopy. The catalog was created with SExtractor (Bertin & Arnouts, 1996), yielding aperture photometry and colours for 1494 sources in the LRIS field of view (Fig. 1). Additional V-, R-, and I-band images centered on RX J0152.7-1357 were obtained with the FORS1 (FOocal Reducer and low dispersion Spectrograph; Appenzeller & Rupprecht 1992) at the ESO VLT and cover a field of view of $6.8' \times 6.8'$ centered. Vega magnitudes are used throughout this paper.

2.2. Spectroscopic observations and data reduction

The spectroscopic observations of RX J0152.7-1357 were conducted in visitor and service modes (VM and SM) from December 1999 to December 2003, as summarized in Table 1. Bayesian photometric redshifts (Benítez 2000) were computed for each source using our BVRIJK_s catalog. Candidates for spectroscopy were selected according to their R-band magnitudes ($R < 24$) and photometric redshifts ($0.7 < z_{\text{phot}} < 0.95$). This photometric redshift interval was chosen to match the dispersion in $z_{\text{phot}} - z_{\text{spec}}$ of the ~ 20 redshifts obtained from the first few masks, which were designed to target galaxies in the cluster red sequence (CRS). Because of the larger FOV of FORS1 compared to the LRIS and SofI fields of view (see Fig. 1), no multi-band photometric information was available for a number of sources outside the dashed rectangle in Fig. 1, and selections in this region were carried out using only the FORS1 imaging.

At $z \sim 0.8$, spectral features such as the [OII]($\lambda 3727$) emission line, the CaII H and K absorption lines and the 4000 Å break, which are normally used to measure the redshift of a galaxy, are between 6500 and 8500 Å. An adequate coverage of this range is provided with the 300I grism of FORS². During poor seeing conditions, we used

¹ Throughout this paper we assume a Λ CDM cosmology with $H_0 = 70 \text{ km s}^{-1} \text{ Mpc}^{-1}$, $\Omega_M=0.3$ and $\Omega_\Lambda=0.7$.

² When we wish to refer to FORS1 and FORS2, we simply write FORS

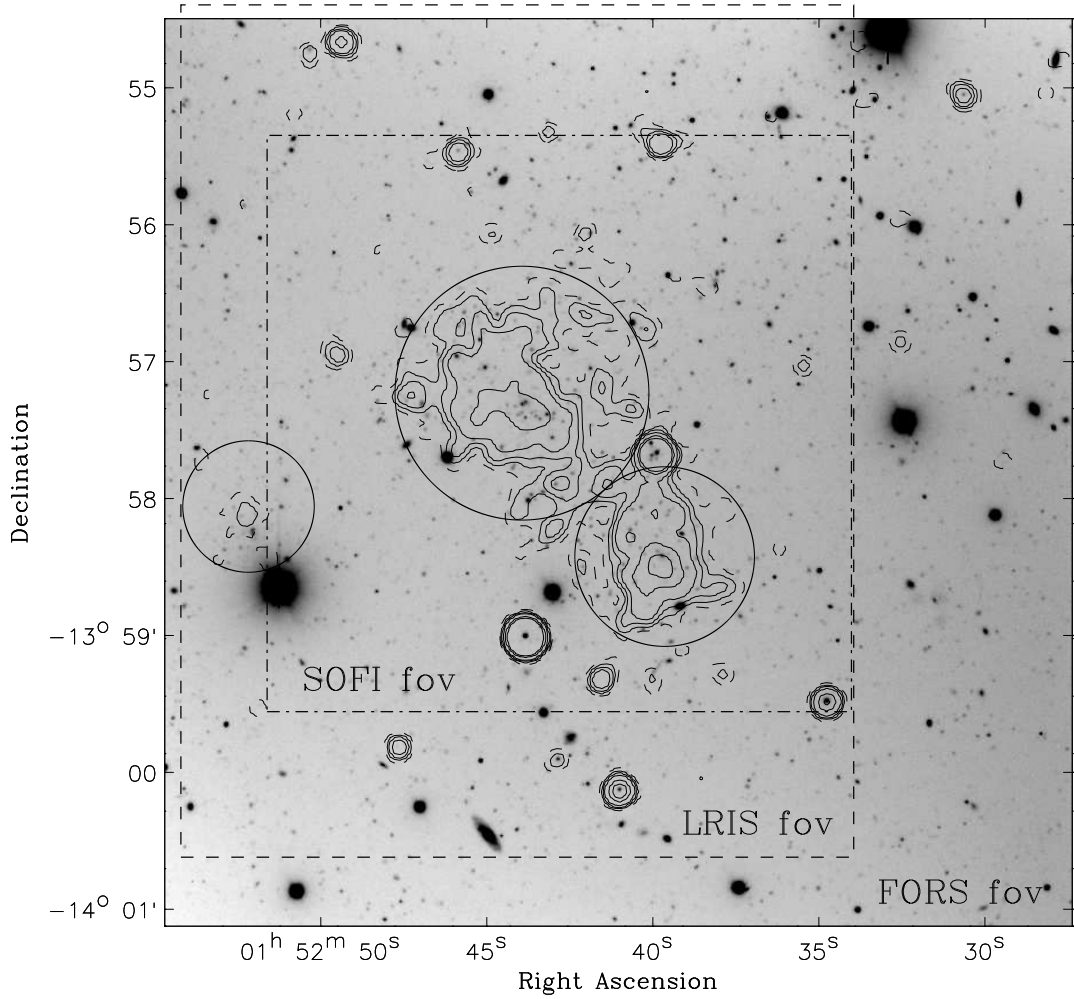


Figure 1 A FORS1 V-, R-, and I-band composite image centered on RX J0152.7-1357. The dashed rectangle corresponds to the $4.9' \times 6.8'$ region covered by the LRIS data superimposed onto the $6.8' \times 6.8'$ field of view (FOV) of FORS1. The dot-dashed square corresponds to $4.9' \times 4.9'$ region covered by SOFI. North is up and East is to the left. Target galaxies selected from the photometric catalog are within the area delimited by the dashed rectangle. Also shown are X-ray Chandra iso-contours, tracing the intracluster medium (ICM) of RX J0152.7-1357, as defined in Fig. 4. The dashed contour corresponds to the 3σ level above the background. Three circular regions, corresponding to regions of extended X-ray emission, have been defined. The radius of each region was defined so that most of the X-ray light within the 3σ iso-contours is contained in the corresponding region (see text for details).

the 150I grism, which provides additional coverage below 5000 \AA , to observe relatively bright field galaxies with a lower resolution. No order-separation filters were used in order to obtain extended coverage in the blue part of the spectrum.

A total of 11 masks for multi-object spectroscopy were prepared with FIMS, the FORS mask preparation tool. Seven masks were designed for use with the MOS (Multi Object Spectroscopy) mode and the other four masks were designed for use with the MXU (Mask Exchange Unit) mode. The MOS mode allows the positioning of up to 19 slits per mask, each of which is $22.5''$ long and formed by

a pair of movable blades. In the MXU mode, each mask contains a larger number of slits, which can be chosen to vary in length. In order to remove fringes accurately (see below), we chose a minimum slit-length of $10''$ allowing us to place up to ~ 40 slits per mask.

MOS observations were carried out with both FORS1 and FORS2 (see Table 1), while the MXU mode was only available with FORS2. Before March 2002, both FORS1 and FORS2 were equipped with Tektronix CCD detectors with 2080×2048 pixels. During March 2002, FORS2 was upgraded with a mosaic of two $2k \times 4k$ MIT CCDs with a gap of $4''$ between them. As a result the sensitivity in the

Mask Name	Date	Telescope	Instrument	Grism/Filter	Exp. Time	No. Exposures	Mask
m6	Dec 1999	UT1	FORS1	300I/none	1800	2	MOS
m1	Oct 2000	UT2	FORS2	300I/none	1800	4	MOS
m2	Oct 2000	UT2	FORS2	300I/none	1800	4	MOS
m3	Oct 2000	UT2	FORS2	300I/none	1800	4	MOS
m4	Oct 2000	UT2	FORS2	300I/none	1800	8	MOS
m5	Oct 2000	UT1	FORS1	150I/none	1800	1	MOS
m7	Nov 2001	UT4	FORS2	300I/none	1800	6	MOS
m8	Aug 2002	UT4	FORS2	300I/none	2030	4	MXU
m9	Aug 2002	UT4	FORS2	300I/none	2030	6	MXU
m10	Sep 2003	UT4	FORS2	150I/none	1200	13	MXU
m11	Sep 2003	UT4	FORS2	150I/none	1200	1	MXU
m11	Nov 2003	UT4	FORS2	150I/none	1200	3	MXU
m11	Dec 2003	UT4	FORS2	150I/none	1200	10	MXU

Table 1 A summary of the VLT spectroscopic survey on RX J0152.7-1357. The first column lists the mask name, the second column lists the observation date, the third column lists the telescope and the fourth column lists the instrument. After August 2002, all the observations were carried out with the FORS2 CCD mosaic. The fifth column lists the grism and the blocking filter used in the observation. The sixth column shows the integration time per exposure and the seventh column shows the number of exposures. The last column lists the mask type (MOS or MXU) used.

red increased by 30%, allowing us to obtain about 30% more redshifts per mask. Our data were taken in the standard resolution mode, which provides a field of view of $6/8 \times 6/8$ arcseconds. Slit widths of 1.0, 1.2, and 1.4 arcseconds were used in MOS observations on both FORS1 and FORS2, which resulted in spectral resolutions of $\sim 13 \text{ \AA}$, $\sim 16 \text{ \AA}$, and $\sim 18 \text{ \AA}$ respectively for the 300I grism, and resolutions of $\sim 27 \text{ \AA}$, $\sim 32 \text{ \AA}$, and $\sim 38 \text{ \AA}$ respectively for the 150I grism. For MXU observations, all slits were $1''$ wide, which corresponds to resolutions of $\sim 28 \text{ \AA}$ and $\sim 13 \text{ \AA}$ for the 150I and 300I grisms respectively. The main characteristics are summarized in Table 2.

During the MXU observations, the targets were dithered along the direction of the slits in order to allow for the removal of fringes in the spectra. This fringing pattern may be quite strong at wavelengths beyond 7000 \AA , complicating the identification of spectral features in the red. Indeed, our first MOS observations with the Tektronix CCD, carried out with no dithering, showed the importance of offsetting the telescope between exposures. With the new FORS2 MIT CCD mosaic; however, the fringe amplitude was determined to be $\lesssim 5\%$. Nevertheless, fringe removal was still needed to reach the Poisson noise limit. Both VM and SM observations were carried out under seeing conditions of $< 0''8$.

To assist in data reduction, we developed a specially dedicated IRAF³ pipeline, which included shell scripts. This pipeline was optimised to reduce data taken with the FORS2 MIT CCD mosaic, controlling the separate reduction of each chip in an interactive way and merging the two reduced frames to produce a final single image. Standard IRAF tasks were implemented to perform bias and flat corrections, and once the single frames corresponding to a given mask were obtained, the slitlets for each exposure

were grouped according to slit number. Single slit spectra were then background subtracted and (when dithered exposures were available) fringe corrected using an algorithm similar to that implemented in BOGUS⁴, which was developed by D. Stern, A.J. Bunker and S.A. Stanford. The sky was subtracted using the standard IRAF routines, and the fringe-corrected and sky-subtracted frames were registered and combined. Extraction, wavelength and flux calibration were carried out in a standard manner. Signal-to-noise ratios varied from values lower than 1, in cases where no continuum but only emission lines were detected, up to values of 50 or more per pixel at about 4000 \AA in the rest frame. At a redshift of $z = 0.84$, the H_δ ($\lambda 4101.7$) absorption feature falls at about 53 \AA from the atmospheric A-band at about 7600 \AA , which was removed with the IRAF task TELLURIC.

Finally, the redshifts were measured using the cross-correlation technique (e.g., Tonry & Davis 1979) implemented in the IRAF task XCSAO (Kurtz et al. 1992). The observed spectra were correlated with templates from Kinney et al. (1996), and the typical errors computed by XCSAO were $\delta z \sim 3 \times 10^{-4}$. Multiple observations of some targets allowed us to estimate total (random+systematic) errors, yielding typical values of $\delta z \sim 8 \times 10^{-4}$.

2.3. The spectroscopic catalog

A total of 262 objects were spectroscopically observed with FORS1 and FORS2 between December 1999 and

³ Image Reduction and Analysis Facility. See <http://iraf.noao.edu/iraf-homepage.html>

⁴ BOGUS is available on line at <http://astron.berkeley.edu/~dan/homepage/bogus.html>

FORS Detector	Scale [arcsec/pix]	Grism 150I		Grism 300I	
		λ_{range} [Å]	Disp. [Å/pix]	λ_{range} [Å]	Disp. [Å/pix]
Tektronix CCD	0.20	4000-10000	5.52	6000-10000	2.59
2k×4k MIT CCD	0.25	4000-10000	6.90	6000-10000	3.24

Table 2 The characteristics of spectroscopic modes used in the survey. For more information, see the FORS User Manual issue 2.6 at <http://www.eso.org/instruments/fors1/userman/index.html>.

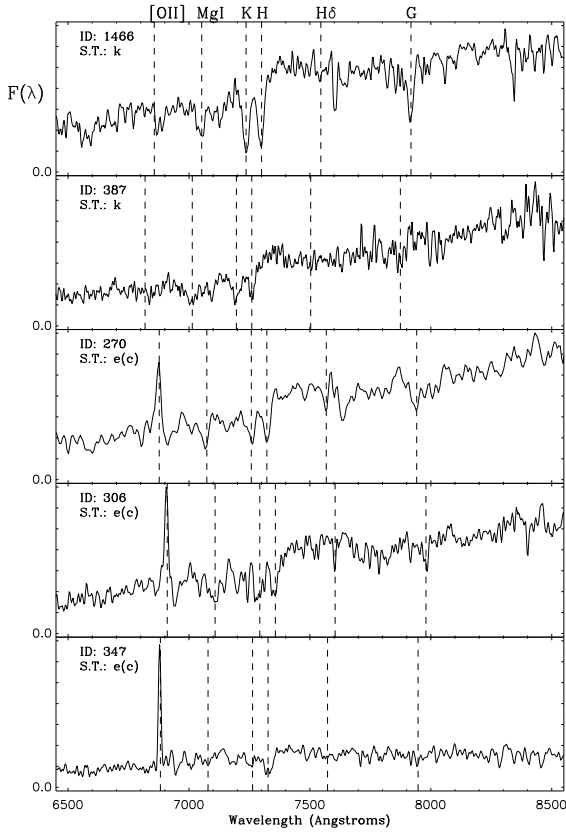


Figure 2 Spectra of five cluster members. The spectra are arranged top to bottom from early type galaxies to late type galaxies. The most common spectral features are indicated by the dashed lines. From left to right they correspond to [OII](λ3727), MgI(λ3834), CaII K(λ3934), CaII H(λ3969), H_δ(λ4102) and the G-band (λ4304). The flux axis is in arbitrary units. The spectroscopic type (S.T.) as defined in Dressler et al. (1999) and the candidate number (ID) are also indicated.

December 2003. We were able to obtain redshifts for 227 (87%) objects, out of which 187 (72%) are secure and 40 (15%) are less secure due to low signal-to-noise.

We classify galaxies as cluster members if they have a secure redshift within $0.81 < z < 0.87$. In this interval, galaxies are within the $\pm 3\sigma_v$ region around the cluster median velocity and the cluster structure appears well isolated in redshift space. The velocity dispersion of RX J0152.7-1357, σ_v , is calculated in section §3.2. With this criterion, 102 objects are classified as cluster members. The corresponding spectroscopic catalog is presented in Table 4. Spectroscopic redshifts and error bars are those computed by XCSAO (Kurtz et al. 1992; see section §2.2).

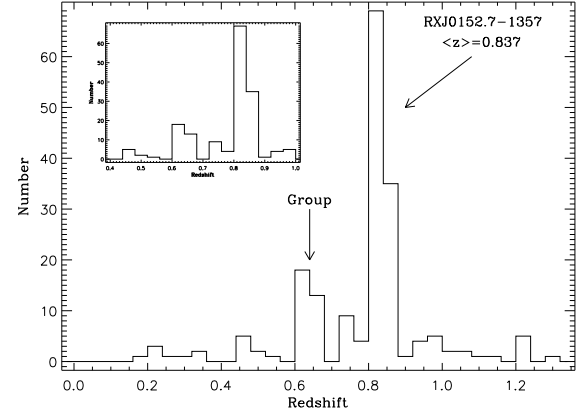


Figure 3 Redshift distribution of 187 galaxies with secure redshifts. The bin size is $\Delta z = 0.04$. The main peak in the distribution corresponds to RX J0152.7-1357 with 102 galaxies within the range $0.81 < z < 0.87$. A secondary peak is observed, indicating the existence of a group of galaxies at $z \sim 0.64$. The inset shows a zoom of the redshift distribution in the $0.4 < z < 1.0$ range.

The most prominent spectral features of each spectrum are indicated in the seventh column of the catalog (Table 4). An emission line flag was given to each object. A value of 0 corresponds to galaxies without observed emission lines, a value of 1 corresponds to galaxies showing any emission line. Two galaxies with broad emission lines (AGNs) were assigned a value of 2. As an example of the data obtained during our survey, the spectra of 5 cluster members are shown in Fig. 2. From top to bottom, the spectra are arranged from early type galaxies to late type galaxies. The galaxy spectroscopic type as defined in Dressler et al. (1999) is also given. The most common spectral features are indicated by dashed lines, as explained in the figure caption.

The number of confirmed cluster members obtained in our spectroscopic survey is comparable to other surveys of distant clusters as, e.g., MS1054-03 (Donahue et al. 1998; Tran et al. 1999; van Dokkum et al. 1999; van Dokkum et al. 2000) and the supercluster Cl 1604+4304 at $z = 0.90$ (Gal & Lubin 2004). In addition to the number of secure members, we have 15 objects at the cluster redshift with less secure redshifts. In Table 5 we also present the coordinates and redshifts of the non-cluster members.

Declination

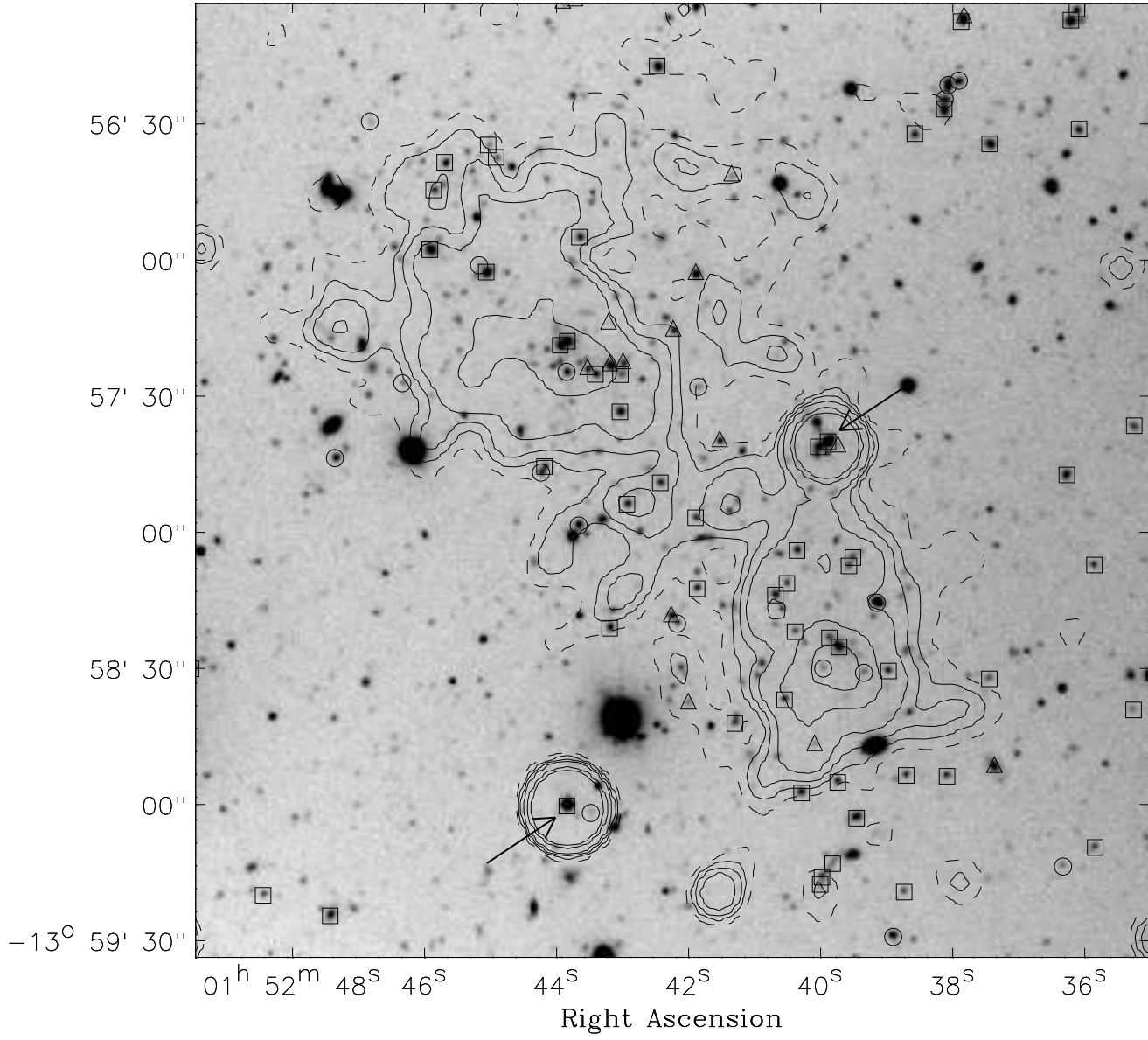


Figure 4 The distribution of confirmed cluster members in the central region of RX J0152.7-1357. The field of view in this figure is $3'5 \times 3'5$ (1.6 Mpc \times 1.6 Mpc at $z \sim 0.84$). North is up and East is to the left. The squares mark the location of cluster members and the contours correspond to X-ray emission (3, 5, 7, 10, 20 and 30 σ above the background in the [0.5-2] keV band) measured with Chandra. The galaxy distribution follows that of the hot intra-cluster gas in the high-density regions. The arrows indicate the location of the two AGNs that are cluster members. Also shown are field galaxies (circles) and galaxies belonging to the foreground group (triangles) at $z \sim 0.64$.

The ground-based photometric catalog itself was used to estimate the success rate of our spectroscopic survey. Since the imaging data were obtained with LRIS, we restrict the analysis to the $4'9 \times 6'54$ field of view of LRIS. We computed the ratio of the number of object with spectroscopic redshifts to the number of objects in the photometric catalogue that were targeted for spectroscopy

as a function of R magnitude. The data were binned in $\Delta R = 0.5$ mag intervals. The ratio is observed to be nearly constant between the interval $20 < R < 24$ with a mean value of 0.89 and a dispersion of 0.07.

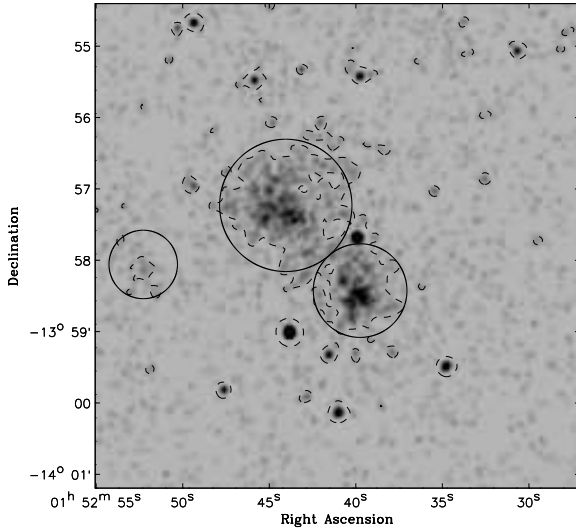


Figure 5 Chandra image of RX J0152.7-1357. The field of view is $6'8 \times 6'8$ and is centered on the cluster, North is up and East is to the left. The dashed contour corresponds to the 3σ level above the background. The circles define the three main regions (northern, southern and eastern clumps) where the extended X-ray emission is greater than 3σ times the background.

3. Analysis

3.1. The survey redshift distribution

Fig. 3 shows the distribution in redshift space of the 202 galaxies for which a secure estimate of the redshift was obtained. The bin size of the histogram was fixed to $\Delta z = 0.04$. RX J0152.7-1357 clearly appears as the most significant structure in the distribution, with a median redshift of $z = 0.837$ (3σ -clipped mean of $\bar{z} = 0.8376 \pm 0.0010$) and 102 galaxies between $z = 0.81$ and $z = 0.87$. All these galaxies are located in the $6'8 \times 6'8$ region covered by FORS1, which is equivalent to an area of $3.1 \text{ Mpc} \times 3.1 \text{ Mpc}$ at the cluster redshift. A secondary peak in the histogram is clearly seen at $z \sim 0.64$, where 31 galaxies have been confirmed in the range $0.60 < z < 0.68$. The spatial distribution of this group of galaxies is quite elongated in the North-South direction, extending across the field of view and passing in front of the cluster as shown in Fig. 4. Its morphology suggests that this structure may be a filament perpendicular to the line of sight, with a projected overdensity of galaxies on top of the northern substructure of RX J0152.7-1357 (see section §3.2). The presence of this foreground structure should be taken into account when estimating the mass of the cluster through the weak lensing technique, which is sensitive to the distribution of matter along the line of sight. No X-ray emission seems to be associated to this structure, indicating that the galaxies in this group do not have a hot gas component.

3.2. Galaxy distribution and substructure in RX J0152.7-1357

The projected distribution of cluster members in the central part of RX J0152.7-1357 is presented in Fig. 4, where cluster members are marked with squares. The X-ray emission, field galaxies (circles) and galaxies belonging to the group at $z \sim 0.64$ (triangles) are also shown. Following the high-density regions as traced by the hot intracluster gas, the cluster members are grouped into two main clumps, one to the north-east of the center of the image (hereafter called northern clump) and the other one to the south-west (hereafter called southern clump). These two clumps are separated by $\sim 1'6$, which corresponds to $\sim 730 \text{ kpc}$ at $z \sim 0.84$, and coincide with the two main peaks observed in the X-ray. Another accumulation of cluster members is observed about $2'4$ ($\sim 1 \text{ Mpc}$ at the cluster redshift) to the East of the central double structure. It is interesting to note that this third clump (hereafter called the eastern clump) also coincides with a region where diffuse X-ray emission is detected with a significance greater than 3σ over the background. These findings clearly support the picture that RX J0152.7-1357 is a dynamically young cluster still in formation, with two and possibly three substructures in an on-going merging phase. Indeed, Maughan et al. (2003) show some evidence for an adiabatic collision in progress between the northern and southern clumps. Additionally, there is an overdensity of cluster members (about 11 galaxies) located to the north-west of the northern clump, although there is no diffuse X-ray emission associated with this clump.

By studying the weak lensing signal around the cluster from HST/ACS data, Jee et al. (2004) find a projected distribution of dark matter (DM) that is in close agreement with both the observed 2-dimensional distribution of galaxies and the ICM in RX J0152.7-1357. The DM map shows a central elongated structure with a strong concentration that coincides with the northern clump. Moreover, the eastern clump is also observed in the weak lensing map, confirming its existence.

The observed substructure in the projected galaxy distribution was also studied in velocity space. We concentrated on substructures that are associated with the diffuse X-ray emission, which were analysed as follows. We separated galaxies located in the northern clump from those located in the southern clump by comparing the Chandra data with the VLT data. Fig. 5 shows a $6'8 \times 6'8$ portion of the Chandra image centered on the cluster. The 3σ level above the background is indicated by the dashed contour. Three circular regions were defined, each centered on one of the three X-ray peaks. The radius of each region was adjusted in order to encompass most of the X-ray emission above the 3σ level. The radii for the northern, southern and eastern clumps are $0'93$ ($\sim 430 \text{ kpc}$), $0'66$ ($\sim 300 \text{ kpc}$), and $0'48$ ($\sim 220 \text{ kpc}$) respectively. Fig. 1 shows the 3σ X-ray iso-contours (dashed

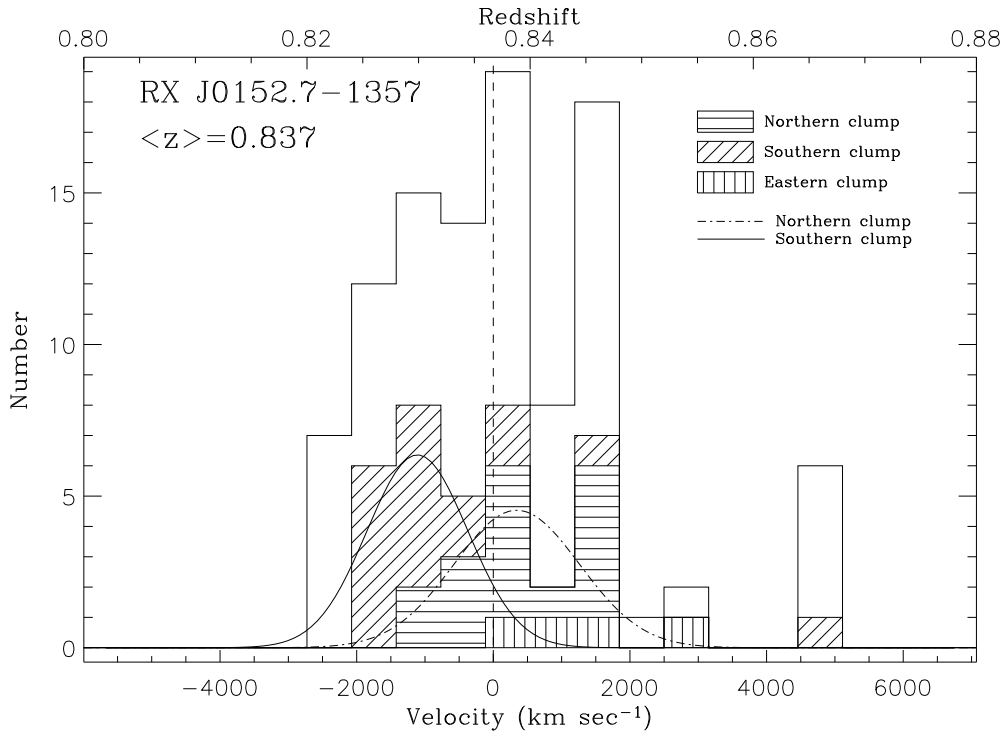


Figure 6 A velocity histogram of the galaxies in RX J0152.7-1357. The unshaded histogram shows the velocity distribution of 102 cluster members, while the shaded histograms correspond to the velocity distributions in the three circular regions encompassing the main substructures. For the sake of clarity, shaded histograms have been stacked instead of overlaid. The two Gaussians represent the distribution of galaxies in the northern and southern clumps. Their location (median redshift) and scale (velocity dispersion) are those given in the text.

curve) and the circular regions overlaid on the FORS1 image. A total of 16 cluster members are located within the circle corresponding to the northern clump, 18 are within the southern clump and 4 are found within the eastern clump. Note that the association of a galaxy to any given clump is based only on the projected distance. The median redshifts of these galaxy clumps are $z_N = 0.8388$, $z_S = 0.8299$ and $z_E = 0.8473$ respectively. The corresponding 3σ -clipped mean redshifts and their standard deviations are: $\bar{z}_N = 0.8390 \pm 0.0013$, $\bar{z}_S = 0.8299 \pm 0.0009$ and $\bar{z}_E = 0.8458 \pm 0.0027$.

The velocity histogram in the cluster rest frame is presented in Fig. 6 (the vertical dashed line corresponds to $z=0.837$). The unshaded histogram shows the distribution of the 102 cluster members, while the shaded histograms correspond to the distributions in the three circular regions defined above and indicated in Fig. 1. For the sake of clarity, the shaded histograms have been stacked instead of overlaid. A close inspection of the velocity histogram shows that the kinematic behavior of the galaxies in the two main clumps are different. Indeed, a large fraction of the galaxies in the southern clump have negative *peculiar* velocities, despite some outliers moving at velocities greater than 2000 km s^{-1} . The northern clump instead has a mean velocity close to the median of the overall velocity distribution. In addition to this, the four galaxies in the eastern clump are observed to have positive *pecu-*

liar radial velocities. Based on Tukey's biweight estimator, we compute the velocity dispersion for the two main galaxy clumps, obtaining $\sigma_N = 919 \pm 168 \text{ km s}^{-1}$ and $\sigma_S = 737 \pm 126 \text{ km s}^{-1}$. These numbers should be taken with caution, because of the small number of redshifts, the simple analysis, and because the distribution of galaxies may be less virialised than the gas, as the ICM is expected to reach an equilibrium state in a shorter time scale compared to galaxies and dark matter particles. Nevertheless, these values are in agreement with what is expected from X-ray temperatures (Wu, Fang & Xu 1998), indicating that the galaxies in these two sub-clumps are probably virialised. Two Gaussians with median redshifts z_N and z_S and velocity dispersions σ_N and σ_S are also shown in Fig. 6 to represent the distribution of galaxies in the northern and southern clumps respectively. A least-squares fit of a Gaussian to all the cluster members was performed, yielding a velocity dispersion of $\sigma_v = 1546 \pm 208 \text{ km s}^{-1}$. A more robust estimate by using the Tukey's biweight estimator delivers a value of $\sigma_v = 1632 \pm 115 \text{ km s}^{-1}$. Assuming a virialised state, a velocity dispersion of $\sigma_v = 1600 \text{ km s}^{-1}$ corresponds to an X-ray temperature of $T_X = 16 \text{ keV}$, which is significantly higher than the observed value, therefore the overall structure of the cluster is not in dynamical equilibrium.

We anticipate that the results obtained in this section are in good agreement with a more specific kinematic anal-

ysis presented in Girardi et al. (in preparation). The latter includes the use of robust statistical indicators (e.g., Beers et al. 1990) to determine velocity dispersions and a formal identification of substructures (e.g., Dressler & Schectman 1988; Mercurio et al. 2003a) in velocity space. We refer the reader to Girardi et al. for a more complete analysis of the kinematical structure of RX J0152.7-1357 and its mass estimate.

3.3. Mass and luminosity estimates

A simple estimation of the mass of the northern and southern subclusters can be obtained from (see e.g. Longair 1998):

$$M(R) = 3 \frac{\sigma_v^2 R}{G} , \quad (1)$$

where G is the gravitational constant and σ_v is the velocity dispersion along the line of sight obtained above. The velocity dispersions σ_N and σ_S (see §3.2) for the northern and southern clumps respectively have been used together with the radii defined for the same substructures, $r_N = 430$ kpc and $r_S = 300$ kpc (see §3.2 and Fig. 1), to estimate their masses via Eq. 1. We find $M_N = (2.5 \pm 0.9) \times 10^{14} M_\odot$ and $M_S = (1.1 \pm 0.4) \times 10^{14} M_\odot$ for the northern and southern subclusters respectively. The sum of these two values gives $M = (3.6 \pm 1.0) \times 10^{14} M_\odot$. These values are in good agreement with the results obtained by Huo et al. (2004) based on a joint analysis of Chandra and Keck data. Our mass estimates for the northern and southern subclusters are also consistent with the mass estimates within r_{500} (the radius within which the mean density is 500 times the critical density of the universe at the given redshift) presented by Ettori et al. (2004) for the same substructures.

It is not simple to make a direct and clean comparison of our mass values to those given in the weak lensing analysis of Jee et al. (2004) and the X-ray study of Maughan et al. (2003). The mass clumps C and F in Jee et al. (2004) correspond to our northern and southern subclusters respectively. Our eastern clump corresponds to mass clump A in the weak lensing map. The mass values in Table 2 of Jee et al. (2004) are given within an aperture of $20''$ (~ 152 kpc) in radius. Within the same aperture, we obtain about 68% less spectroscopically confirmed galaxies in the main central clumps than those reported above (see §3.2), for which our velocity dispersion and therefore mass estimates would not be reliable. However we note that the mass value of $(2.1 \pm 0.3) \times 10^{14} M_\odot$ obtained by Jee et al. (2004) within an aperture of $50''$ (~ 380 kpc) in radius centered on the northern clump is in very good agreement with our mass estimate given above for the same substructure. Apertures with radii larger than r_N and r_S would not be adequate to measure the mass of the northern and southern clumps respectively since they would also include galaxies outside the selected substructure, affecting thus its mass estimate. Therefore we do not compare

masses to those in Jee et al. (2004) and Maughan et al. (2003) computed within 1 Mpc and 1.4 Mpc radius apertures. However, we note that the value of $2.4_{-0.3}^{+0.4} \times 10^{14} M_\odot$ in Maughan et al. (2003), obtained from combining the masses of the two subclusters within apertures of about $50''$ (~ 380 kpc) are in good agreement, within the uncertainties, with our combined mass of the northern and southern subclusters given above.

Since the overall galaxy distribution in RX J0152.7-1357 is not in virial equilibrium, our velocity dispersion value from the 102 spectroscopically confirmed cluster members leads us to overestimate the true total mass of the cluster. Considering an aperture of $R = 1$ Mpc our value of $\sigma_v = 1632 \pm 115$ km s $^{-1}$ yields a $M_{CL} = (1.9 \pm 0.3) \times 10^{15} M_\odot$, about 4 times larger than the value obtained from the weak lensing analysis (Jee et al. 2004) within the same aperture. From Eq. 1, the mass within the virial radius of $R=1.4$ Mpc (see Maughan et al. 2003) associated to the same value of σ_v turns out to be $M_{CL} = (2.6 \pm 0.4) \times 10^{15} M_\odot$, about within a factor of two of the combined total mass of the two subclusters extrapolated to the virial radius in Maughan et al. (2003) paper.

Our ground based I-band photometry was used to estimate the total luminosity in the B-band, L_B , from the cluster galaxies within a given aperture. The large number of spectroscopically confirmed cluster members, which are likely to be the bright ones and thus dominate the total optical cluster light, allow us to make a fair estimate of L_B . By using the galaxy templates in Benítez et al. (2004) and following the procedure described in Cross et al. (2004) to compute rest-frame B-band magnitudes, B_{rest} , we obtain the transformation from our I-band photometry to the B_{rest} magnitudes to be $B_{rest} = I - dm - k_{BI}$, where dm is the distance modulus of the cluster and k_{BI} is the general k -correction term computed from the template galaxy spectra. This depends on the B- and I-band filters and redshift. At the cluster redshift of $z = 0.837$ we obtain values of $dm = 43.62$ and $k_{BI} = -1.35$, the latter being only weakly dependent on galaxy type. The total B-band luminosity is then computed as:

$$\frac{L_B}{L_{B,\odot}} = \sum_j 10^{0.4 \{ M_{B,\odot} - B_{rest,j} \}} , \quad (2)$$

where $M_{B,\odot} = 5.48$ is the absolute B magnitude of the sun, $L_{B,\odot}$ is the solar luminosity in the B band and the sum is extended to all the objects within the given aperture. In order to compare our results with those from the weak lensing analysis, we compute L_B within an aperture of 1 Mpc centered on the northern clump. From Eq. 2 we obtain $L_B = 4.8 \times 10^{12} L_{B,\odot}$, which is in excellent agreement with the value of $L_B = 5.2 \times 10^{12} L_{B,\odot}$ given in Jee et al. (2004). However, since we only considered spectroscopically confirmed members, our value of L_B may be underestimated.

As was the case in comparing mass estimates, a direct and clean comparison of the mass-to-light ratios obtained

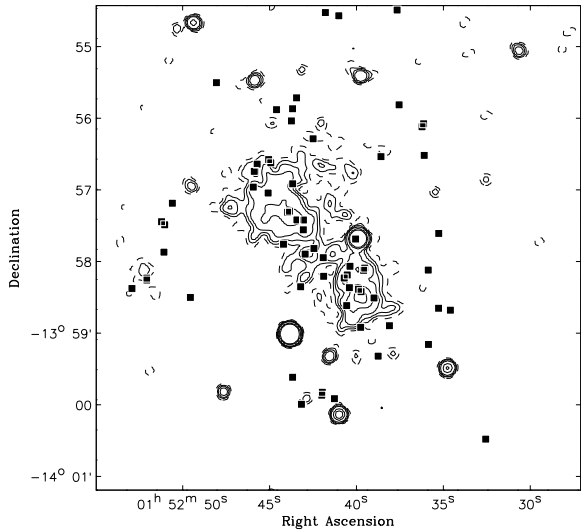


Figure 7 The projected distribution of cluster members without emission lines (filled squares). X-ray iso-contours are also shown.

in this paper for the northern and southern clumps to the values given in the weak lensing paper (Jee et al. 2004) cannot be done. Within our apertures of $r_N = 430$ kpc and $r_S = 300$ kpc in radius we obtain mass-to-light ratios of $(246 \pm 89)M_\odot/L_{B,\odot}$ and $(152 \pm 55)M_\odot/L_{B,\odot}$ for the northern and southern subclusters respectively. As a reference, the M/L_B value obtained by Jee et al. (2004) within a 1 Mpc aperture centered on the northern clump is $(92 \pm 7)M_\odot/L_{B,\odot}$, significantly lower than our values for any of the main subclusters. However, since we only count spectroscopically confirmed cluster members, it is possible that we are missing some of the B-band light from unconfirmed cluster galaxies and that we are likely overestimating the M/L_B ratios. Our value of M/L_B for the northern clump is about 1.8 times higher than the expected one from the mass-to-light ratio profile presented in Fig. 19 of Jee et al. (2004).

3.4. Galaxy populations and substructure

We use the spectra to divide cluster members into two subsets: those with emission lines (star-forming galaxies) and those without clear emission lines (passive galaxies). Figures 7 and 8 show the projected distribution of these subsets. In our spectroscopic sample of cluster members, 34 (33%) cluster members, excluding the 2 AGN, have clear emission line features, such as [OII] ($\lambda 3727$) or

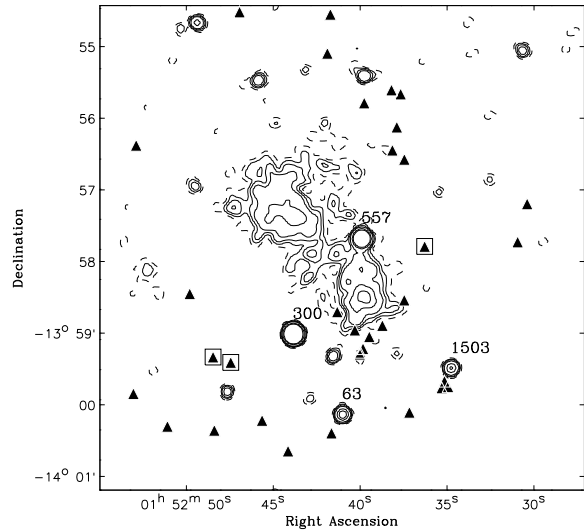


Figure 8 The projected distribution of cluster members with emission lines (filled triangles). X-ray iso-contours are also shown. Open squares indicate the location of red star-forming galaxies. The spectroscopically observed AGN are labeled with their corresponding IDs and their redshifts are given in Table 3.4.1.

[OIII] ($\lambda 5007$), indicating the existence of on-going star-formation.

The three high-density regions in the cluster mass distribution, as traced by the hot X-ray gas (see Fig. 5), are populated by passive galaxies exclusively. All the star-forming galaxies noticeably avoid these regions. A few galaxies with narrow emission lines are observed close to the southern edge of the southern clump (see Fig. 8). These galaxies are about $30''$ (~ 230 kpc) from the centroid of the southern X-ray substructure, which corresponds to a region where the local ICM density is about one-third of the central density of the southern clump, as derived from the X-ray surface brightness profile.

In terms of spectral classification, passive galaxies are split into two main groups: k type galaxies (see Dressler et al. 1999; Poggianti et al. 1999) and post-starburst galaxies (Dressler & Gunn 1983), also called “E+A” galaxies. Based on the strength of the $H_\delta(\lambda 4102)$ line, post-starburst galaxies can be further divided into k + a and a + k type galaxies. (Franx 1993; Dressler et al. 1999; Poggianti et al. 1999). Northern, southern and eastern clumps are mostly populated by k type galaxies and a few k + a and a + k galaxies are also seen in these clumps. The classification as post-starburst galaxies of two out of ten cluster members may be uncertain due to the possible alteration of the H_δ equivalent width by the telluric correction.

Most passive galaxies have red colours ($R - K_s \simeq 5$) and most of them populate the cluster red sequence (CRS) in the colour-magnitude diagram (CMD). In Fig. 9, we show the distribution of cluster members that have ground

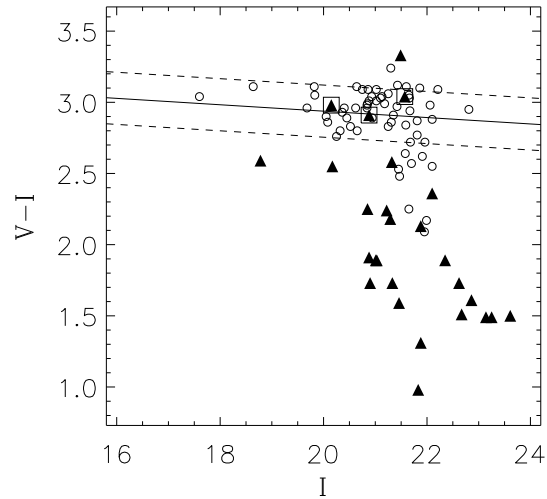
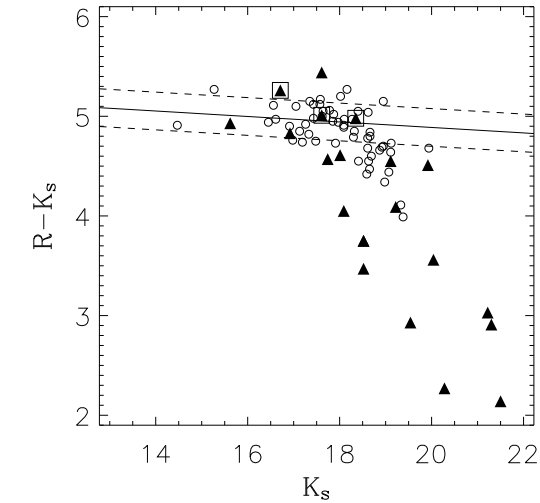


Figure 9 Colour-Magnitude diagrams of cluster members within the LRIS field of view. Open circles are passive galaxies and solid triangles are star-forming galaxies. The solid line corresponds to a linear fit to the data within the cluster red sequence (CRS) defined as the $[14 < K_s < 18.5, 4.5 < R - K_s < 6]$ region in the upper panel and the $[16 < I < 22, 2.3 < V - I < 3.5]$ region in the lower panel. Dashed lines indicate the $1-\sigma$ level above and below the linear fit ($\sigma = 0.19 \pm 0.02$ in upper panel and $\sigma = 0.18 \pm 0.02$ in lower panel). The large scatter is in part due to the shallowness of our ground based photometry. The reddest galaxies with narrow emission lines in the Colour-Colour diagrams of Fig. 10 are indicated by open squares.

based LRIS and SofI photometry in two CMDs. Open circles are passive galaxies and solid triangles are star-forming galaxies. The solid lines correspond to linear fits ($R - K_s = -0.027 K_s + 5.44$ in upper panel and

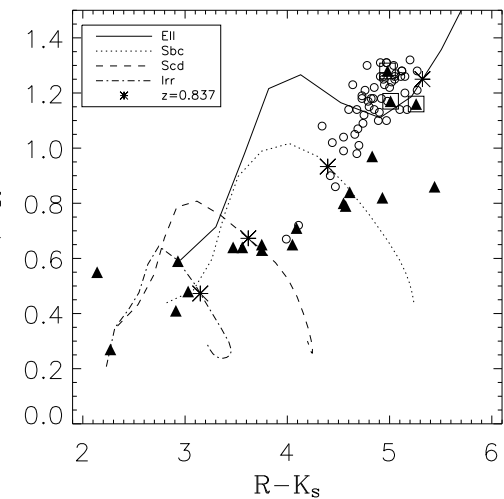
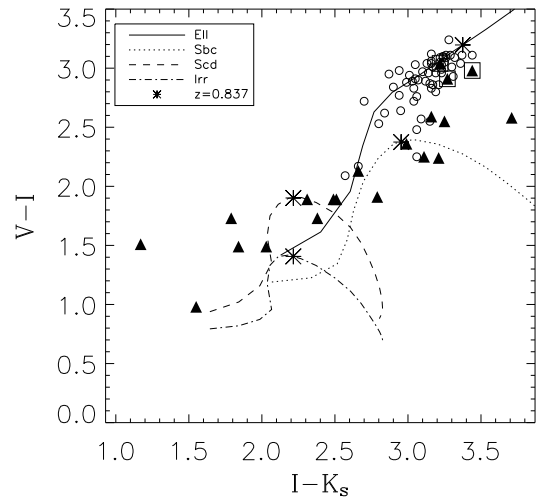


Figure 10 Colour-Colour diagrams of cluster members within the LRIS field of view. Open circles are passive galaxies and solid triangles are star-forming galaxies. The reddest galaxies with narrow emission lines are indicated by open squares. Colour-colour tracks based on model spectra of Ell, Sbc, Scd and Irr galaxies without evolution are also shown. Expected colours for the different galaxy types at the cluster redshift are indicated with stars.

$V - I = -0.022 I + 3.39$ in lower panel) to the data within the regions defined in the caption of Fig. 9. Dashed lines indicate the $1-\sigma$ level above and below the fits. If we compare the CRS of the $R - K_s$ vs K_s diagram to the models computed by Kodama & Arimoto (1997), we infer that the colours of the passive galaxies in the CRS are consistent with an early formation epoch ($z \gtrsim 2$). However, we note the presence of a tail of fainter ($K_s \gtrsim 18.5$) passive galaxies extending to bluer ($4.0 \lesssim R - K_s \lesssim 5.7$) colours, off the

CRS. Passive galaxies are also observed outside the high-density peaks, however the outskirts of RX J0152.7-1357 are dominated by star-forming galaxies.

The segregation between star-forming and passive galaxies in RX J0152.7-1357 is in agreement with a picture in which the star formation activity in galaxies is suppressed during the infall of these galaxies into the highest density zones. An analysis of the physical properties of the star-forming galaxy population in RX J0152.7-1357 based on the combination of VLT spectroscopic and HST/ACS imaging data, together with implications for cluster galaxy evolution, will be presented in Homeier et al. 2004.

In Fig. 10, we show the distribution of cluster members in two colour-colour diagrams. The symbols are the same as those in Fig. 9. For reference, we also show the tracks as a function of redshift for an elliptical (Ell) and three late-type (Sbc, Scd and Irr) galaxies using the template library of Coleman, Wu, & Weedman (1980), whose spectral energy distributions (SEDs) have been extended to the near-IR and far-UV using Bruzual & Charlot (1993, with recent updates) models. The tracks include k-corrections only. The expected colours for the different galaxy types at the cluster redshift are indicated with stars. Passive galaxies are located in the upper right part of both colour-colour diagrams (see Fig. 10). The observed offset between the locus of these galaxies and their expected colours from the models is consistent with passive evolution of early-type galaxies formed at $z \sim 1.9$.

Finally, we note that the brightest cluster member of the southern clump (ID=387) is redder than the brightest cluster member of the northern clump (ID=701). The differences in the colours are $\Delta(R - K_s) = 0.17$ and $\Delta(V - I) = 0.15$ with errors of $\delta(R - K_s) = 0.015$ and $\delta(V - I) = 0.012$ respectively. These differences in colour get bigger if we compare ID=387 with the pair of bright galaxies (ID=1466 and ID=1467) located in the core of the northern clump. Galaxy ID=387 turns out to be ~ 0.25 magnitudes redder in $R - K_s$ and ~ 0.24 magnitudes redder in $V - I$ than both galaxies at the core of the northern subcluster. Assuming that these galaxies have similar metallicities, such a difference in colour may be an indication of a difference in stellar ages. However, more accurate photometry, such as, e.g., ACS photometry, would be needed to confirm this result (Blakeslee et al., in preparation).

3.4.1. Red star-forming galaxies

Although most of the star-forming galaxies are seen to populate the lower right region of the CMD, there are a few that are located in the RCS and in the locus occupied by early-type galaxies in the colour-colour diagrams in Fig. 10. The three reddest galaxies with emission features are indicated by open squares (see Figs. 9 and 10) and represent about 5% (3 out of 64) of the galaxies within the CRS. Their red colours ($R - K_s \simeq 5$) suggest that

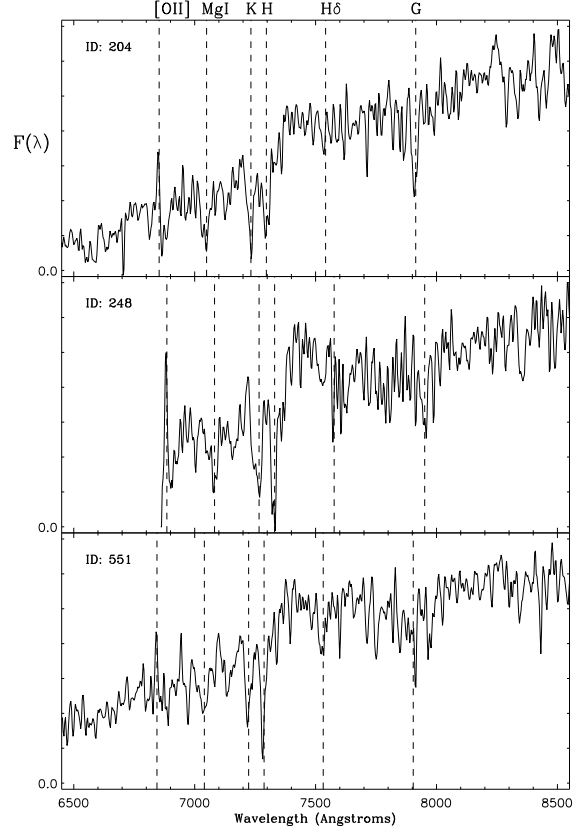


Figure 11 Spectra of red star-forming galaxies. The ID number of the shown spectra are, from top to bottom: 204, 248 and 551. Important spectral features are indicated with dashed lines (for a comparison, see Fig. 2). The flux is in arbitrary units. Due to the location of galaxy 248 in the mask, there is no data for wavelengths blueward of the [OII] ($\lambda 3727$) line.

these galaxies are dominated by an old stellar population, although dust extinction can significantly affect the observed colours. The spectra of these galaxies are shown in Fig. 11. In addition to the [OII] ($\lambda 3727$) emission line observed in their spectra, 2 of these galaxies show a prominent H_δ ($\lambda 4102$) feature in absorption, indicating the existence of a coeval young stellar population (~ 1 Gyr). In the case of galaxy ID=248, H_δ ($\lambda 4102$) lies at about 23 Å from the subtracted A-band feature which may have introduced an uncertainty of $\sim 20\%$ in its equivalent width after the A-band subtraction procedure.

A measurement of the CaII H + He to CaII K ratio (Rose 1984, 1985) indicates that galaxies ID=248 and ID=551 have a significant post-starburst component. In the case of galaxy ID=204, the CaII H + He to CaII K ratio turns out to be inconsistently larger than the observed index values for different MK spectral types (Rose 1985). As observed in the 2-d spectrum of this object, the inconsistency may be due to a sky line effecting the CaII K line. These galaxies host a mixture of old and young stellar populations together with on-going star formation. Our ground-based imaging does not allow us to securely determine the morphology of these galaxies, but

the spectral energy distribution (SED) and the spectral features suggest that they may be Sa-Sb type galaxies. In terms of spectral classification, these galaxies have a k + a spectrum (Franx 1993) with [OII] superposed. Based on the equivalent widths of [OII] and H_δ only, these galaxies may be classified as e(c) (Poggianti et al. 1999). However, their colours are redder than e(c) galaxies and as red as k type galaxies. Therefore we have decided to classify them as a + k + [OII] (Table 4) to denote their star-forming nature as well as their red colour and the post-starburst component.

Similar to the other star-forming galaxies in RX J0152.7-1357, these red star-forming galaxies are located in the outskirts of the cluster (see Fig. 8). They are also spatially isolated. The reddest emission line galaxy in the $R - K_s$ vs K_s diagram of Fig. 9 is galaxy ID=270, which has a disturbed, elongated morphology. In contrast to the other three red star-forming galaxies, its prominent [OII] ($\lambda 3727$) line is likely to be due to star-formation activity induced by a possible interaction.

The observation of red star-forming galaxies in the field environment has already been reported in previous works (e.g., Graham & Dey 1996; Afonso et al. 2001; Cimatti et al. 2002). Galaxies with red SEDs and emission lines have been observed in the Canada-France Redshift Survey (Hammer et al. 1997), and 8% of these galaxies at $z < 0.7$ can be places of a vigorous star-formation activity affected by strong dust absorption. In the cluster environment, on the other hand, Duc et al. (2002) found that about 9% of galaxies in the CRS of Abell 1689, have a star-formation activity which is mainly detected by their observed flux at $15 \mu\text{m}$, with all but one of these galaxies showing no measurable [OII] ($\lambda 3727$). This indicates that most of the star-formation activity in this $z = 0.18$ cluster is hidden. These obscured star-forming galaxies have projected distances within 550 kpc from the center of the cluster. In addition to this, all but one of the star-forming galaxies in the CRS of Abell 1689 are classified as k type (Poggianti et al. 1999). At lower redshift, the CMD of the Virgo cluster presented by Gavazzi et al. (2002) shows that some luminous spiral galaxies have colours as red as cluster ellipticals, however no explicit indication of their star-forming nature is given.

Although no red k + a with [OII] galaxies have been reported in the distant cluster MS1054 (e.g., van Dokkum et al. 2000) or the super cluster Cl 1604+4304 (e.g., Postman, Lubin & Oke 1998; Gal & Lubin 2004), there is evidence that some galaxies with these peculiar spectro-photometric characteristics have indeed been detected in RDCS J0848+4453 (van Dokkum & Stanford 2003), a cluster at $z=1.27$ in the Lynx field (Stanford et al. 1997; Rosati et al. 1999). Two of the three galaxies presented in van Dokkum & Stanford (2003) have prominent [OII] ($\lambda 3727$) in emission, accompanied by some evidence for enhanced H_δ ($\lambda 4102$) in absorption. These galaxies have $I - H > 3$ colours and, in contrast to RX J0152.7-1357, are observed in the central $1.1 \text{ Mpc} \times 1.1 \text{ Mpc}$ region of RDCS J0848+4453. The X-ray morphology of RDCS

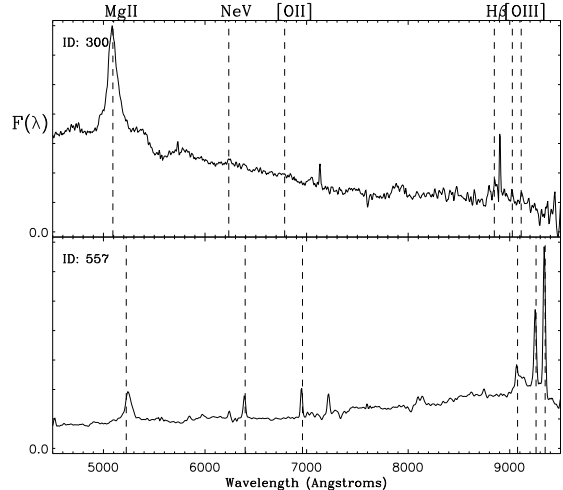


Figure 12 Spectra of the two AGNs that are cluster members. The flux is in arbitrary units. From top to bottom the AGNs are at $z=0.8201$ (ID=300) and $z=0.8672$ (ID=557). The dashed vertical lines indicate some important emission features. From left to right these are MgII ($\lambda 2798$), NeV ($\lambda 3425$), [OII] ($\lambda 3727$), H_β ($\lambda 4861$), [OIII] ($\lambda 4959$) and [OIII] ($\lambda 5007$).

J0848+4453 (Stanford et al. 2001) is as irregular as that of RX J0152.7-1357. However, the X-ray morphologies of MS1054 (Gioia et al. 2004) and Cl 1604+4304 (Lubin, Mulchaey & Postman 2004) are also irregular, so a connection between the existence and location of this type of galaxy in a cluster and the cluster dynamical state is not clear.

The observation of galaxies with a mixture of stellar populations in a forming cluster at high redshift represents a key point in the study of galaxy evolution, since these galaxies may be transition objects between field spirals and cluster elliptical galaxies.

3.5. X-ray point sources

The high angular resolution of Chandra has allowed us to identify for the first time a number of X-ray point sources in the FORS1 field of RX J0152.7-1357. Previous observations of RX J0152.7-1357 with ROSAT and BeppoSAX (Della Ceca et al., 2000; Romer et al., 2000; Ebeling et al., 2000) were unable to disentangle some of these X-ray point sources from the diffuse emission from the ICM, due to the limited spatial resolution of those satellites. Four of the point sources were targeted during our survey, and all of them are AGNs.

Two of the four AGNs (ID=300 and ID=557), with redshifts of $z=0.8201$ and $z=0.8672$ respectively, are cluster members. One AGN, ID=300, is located ~ 1.16 (~ 530 kpc) to the southeast of the brightest cluster galaxy in the southern clump (ID=387). The other AGN, ID=557, is located $\sim 46''$ (~ 350 kpc) north of ID=387 on the line divid-

ID	α (h:m:s) (J2000)	δ ($^{\circ}:\prime:\prime$) (J2000)	z	$f_X^{(*)}$ [0.5-2] keV	$L_X^{(**)}$ [0.5-2] keV	$f_X^{(*)}$ [2-10] keV	$L_X^{(**)}$ [2-10] keV
300	01:52:43.738	-13:59:01.39	0.8201	3.5097	1.0540	3.5989	1.2777
557	01:52:39.780	-13:57:40.10	0.8672	1.6961	0.1529	7.6439	1.9623
63	01:52:40.915	-14:00:09.72	0.9934	0.5546	0.2362	1.1461	0.4696
1503	01:52:34.676	-13:59:30.54	0.7439	0.3881	0.0492	0.9492	0.2043

Table 3 X-ray fluxes and luminosities of the spectroscopically observed AGN in the FORS1 field of view of RX J0152.7-1357. The first two objects are confirmed cluster members, the other two are field AGNs. All fluxes were computed assuming no intrinsic absorption and a galactic absorption of $n_{H,gal}=1.54 \times 10^{22} \text{ cm}^{-2}$ frozen. The spectral slopes, $\gamma=1.8-2$, are typical for type-1 AGN. Errors ($1-\sigma$) on L_X are of 20%, 25%, 22% and 70% for IDs 300, 557, 63 and 1503 respectively. (*): Fluxes are in units of $10^{-14} \text{ erg s}^{-1} \text{ cm}^{-2}$. (**): Luminosities are in units of $10^{44} \text{ erg s}^{-1}$.

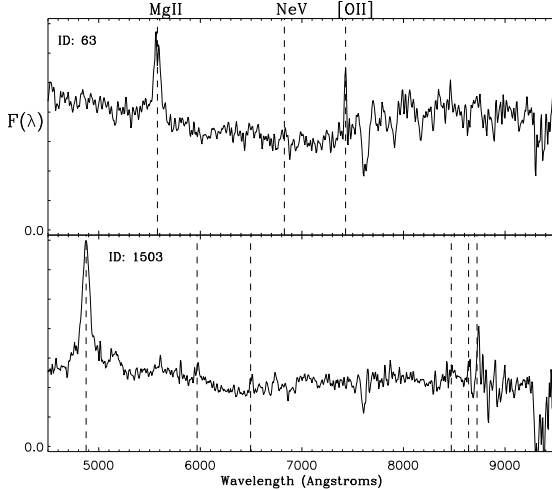


Figure 13 Spectra of the two AGNs that are not cluster members. The flux is in arbitrary units. From top to bottom the AGN are at $z=0.993$ (ID=63) and $z=0.7439$ (ID=1503) respectively. The dashed vertical lines indicate some important emission features (same as in Fig. 12).

ing the two main interacting clumps. The location of these AGNs is indicated by the arrows in Fig. 4. The number of net counts in the [0.5-10] keV band are 314.4 and 233 for ID=300 and ID=557 respectively. Their X-ray fluxes and luminosities obtained from the spectroscopic analysis of the Chandra data are given in Table 3.4.1. The spectra are shown in Figure 12 and both have a prominent broad MgII ($\lambda 2798$) emission line characteristic of AGN.

It is interesting to note the presence of several AGN in the cluster field of view and the fact that the two X-ray point sources closest to the central double core region are also cluster members. These observations are consistent with a picture in which AGN are considered tracers of large scale structures in the universe (e.g., Gilli et al. 2003), however they tend to avoid the central regions of clusters. More AGN identifications around clusters are needed to bridge the gap between moderate density environments (filaments) and high-density regions (clusters).

The other two AGNs (ID=63 and ID=1503 in Table ?? and Fig. 8) have redshifts of $z=0.9934$ and $z=0.7439$, respectively, and are not cluster members. Their net counts

in the [0.5-10] keV band are 53.197 and 44.019 respectively. Their X-ray fluxes and luminosities are given in Table 3.4.1.

The cluster X-ray flux measured by ROSAT PSPC in the [0.5-2] keV band within a 3 arcmin radius aperture is $f_x = (2.2 \pm 0.2) \times 10^{-13} \text{ erg s}^{-1} \text{ cm}^{-2}$ (Della Ceca et al. 2000). The four X-ray point sources reported in this section are located within the above aperture, however ID=1503 was masked out in the PSPC flux estimation (Della Ceca et al. 2000). From the X-ray fluxes presented in Table 3.4.1, we estimate that the ROSAT flux of RX J0152.7-1357 in the [0.5-2] keV band was overestimated by about 35% due to contamination from the other three AGNs.

4. Discussion and Conclusions

The extensive spectroscopic survey that we have carried out on RX J0152.7-1357 allows us to firmly characterize its dynamical state. The coverage of the cluster field was performed in the most uniform possible manner, allowing us to spectroscopically confirm 102 cluster members. The picture derived from this sample confirms previous findings from X-ray observations. Cluster galaxies are observed to form substructures that coincide with those in the extended X-ray emission. Furthermore, weak lensing data based on ACS imaging (Jee et al. 2004) show that the three major clumps of baryons (hot gas and galaxies) are associated to three separated dark matter halos.

The simple analysis of the cluster galaxy distribution in velocity space presented in section §3.2 gives a velocity dispersion of $\sim 1600 \text{ km s}^{-1}$ to the whole cluster structure. This value is somewhat higher than that measured for MS1054 (Tran et al. 1999) at $z=0.833$ and almost the same, within the uncertainties, to the one measured for RX J1716.6+6708 (Gioia et al. 1999), another dynamically young galaxy cluster at $z=0.81$. This overall velocity dispersion turns out to be larger than that expected from the $\sigma - T$ relation, indicating the unrelaxed state of the cluster. The same analysis allowed us to estimate the velocity dispersion for both the northern and southern clumps, which are in agreement with the observed $\sigma - T_X$ (Wu, Fang & Xu 1998) and $L_x - \sigma$ (Xue & Wu 2000) relations for clusters. In terms of total cluster mass, it is

not possible to give a reliable estimate based on the observed velocity dispersion due to the unvirialised state of the cluster. Numerical simulations (see Roettiger, Loken & Burns 1997) show that mergers make the gas evolve differently from the dark matter, affecting the hydrostatic equilibrium of the gas and, therefore, the dynamical mass estimates based on the cluster X-ray emission as well. The evidence presented in this work as well in others (Maughan et al. 2003; Jee et al. 2004) shows that this is the case for RX J0152.7-1357. In fact, the predicted $M - \sigma$ relation for galaxy clusters (Bryan & Norman 1998) is unable to reconcile the weak lensing mass (Jee et al. 2004) with the overall velocity dispersion presented in this paper. A velocity dispersion of about 1600 km s^{-1} would correspond to a virial mass more than a factor of two greater than the weak lensing measurement. In the case of the northern and southern subclusters, our mass estimates from Eq. 1 are in close agreement, within the uncertainties, with those from the weak lensing and X-ray analyses for the same substructures and within apertures of $\sim 400 \text{ kpc}$ in radius.

The spectrophotometric information of a significant fraction of galaxies down to $\sim R^* + 1$ has allowed us to characterize the galaxy populations in RX J0152.7-1357. In terms of spectroscopic classification, we found the expected spectral type-density relation. The high density regions of the cluster are dominated by red passive galaxies, most of them classified as k type. The lower density regions in the cluster periphery, on the other hand, are dominated by star-forming [OII] galaxies. All galaxies showing on-going star-forming activity clearly avoid the high-density regions as traced by the X-ray gas. We note that star-forming galaxies that are the closest to the central double core structure of RX J0152.7-1357 are located at $\sim 230 \text{ kpc}$ away from the center of the southern clump. This distance is consistent with the location at which starvation (slow decrease in the star formation rate due to ram-pressure stripping, thermal evaporation or turbulent and viscous stripping) starts to become important (see Treu et al. 2003, and references therein).

An important result is the observation of a subpopulation of galaxies belonging to the cluster red sequence ($R - K_s \simeq 5$) which are characterized by the presence of a post-starburst stellar population together with on-going star-formation. Such galaxies, composed of a mixture of stellar populations of different ages, point toward a complex galaxy evolution in such a massive forming cluster. These red star-forming k + a galaxies may be a transition stage from late-type field galaxies to early-type galaxies in high-density regions. Galaxies with post-starburst and on-going star-formation spectral features have been observed in the core of the distant cluster RDCS J0848+4453 ($z = 1.27$; van Dokkum & Stanford 2003), however the strength of the [OII] and Balmer-line features in the spectrum of galaxies ID=248 and ID=551 indicate that more extensive star-forming activity may be occurring in a disk structure. These red star-forming galaxies might represent a cluster elliptical caught in the act of formation. The link

between this population and the dynamical stage of the cluster is something that requires further investigation.

We conclude that the velocity dispersion estimates, indicate that RX J0152.7-1357 is a massive system already in place when the universe was 6.46 Gyr old (48% of its present age). The combination of all the data available on RX J0152.7-1357 leads us to conclude that in this system the dark matter and the baryons trace each other very well, indicating an advanced stage of thermalisation in the cluster potential well. The filamentary structure observed in the RX J0152.7-1357 galaxy distribution agrees well with the X-ray distribution of its ICM. There is strong evidence for significant substructure in this system, with two major sub-clusters in a merging phase. RX J0152.7-1357 shows hierarchical structure formation caught in the act, indicating that large structures are produced by the merging of subunits in the earlier phases of evolution, as expected from the classical picture of hierarchical clustering. RX J0152.7-1357 is an ideal laboratory, where processes affecting galaxy formation are ongoing. It provides us with an opportunity to improve our understanding of galaxy evolution in clusters.

Acknowledgements. This work would not have been possible without the dedicated efforts of ESO staff, in both Chile and Europe. R.D is grateful to Drs. H. Flores and N. Cross for interesting and useful discussions. We are grateful to Dr. Tadayuki Kodama for providing us with a copy of his models and to Dr. John Blakeslee for useful comments and for kindly running galaxy evolution models. We are grateful to the anonymous referee for helpful comments. We wish to acknowledge the great cultural and spiritual role that the summit of Mauna Kea has within the indigenous Hawaiian community and express our gratitude for permission to observe from its summit. We are grateful to the Keck observatory staff for the support during the observations. The W. M. Keck observatory is a scientific partnership between the University of California and the California Institute of Technology, made possible by the generous gift of the W. M. Keck Foundation.

References

- Afonso, J. et al. 2001. ApJL, 559, 101.
- Appenzeller, I. & Rupprecht, G. The ESO Messenger, March 1992. p.18.
- Beers, T. C. et al. 1990. AJ, 100, 32.
- Benítez, N. 2000. ApJ, 536, 571.
- Benítez, N. et al. 2004. ApJS, 150, 1.
- Bertin, E. & Arnouts, S. 1996. A&AS, 117, 393.
- Bryan, G. L. & Norman, M. L. 1998. ApJ, 495, 80.
- Bruzual A., G. & Charlot, S. 1993. ApJ, 405, 538.
- Cimatti, A. et al. 2002. A&A, 381, L68.
- Coleman, G. D., Wu, C. & Weedman, D. W. 1980. ApJS, 43, 393.
- Cross, N. J. G., et al. 2004. AJ, in press.
- Della Ceca, R. et al. 2000. A&A, 353, 498.
- Donahue, M. et al. 1998. ApJ, 502, 550.
- Dressler, A. & Gunn, J. E. 1983. ApJ, 270, 7.
- Dressler, A. & Schectman, S. 1988. AJ, 95, 985.
- Dressler, A. et al. 1999. ApJSS, 122, 51.
- Duc P.-A. et al. 2002. A&A, 382, 60.

Ebeling, H. et al. 2000. *ApJ*, 534, 133.

Ettori, S. et al. 2004. *A&A*, 417, 13.

Franx, M. 1993. *ApJL*, 407, 5.

Gal, R. R. & Lubin, L. M. 2004. *ApJL*, 607, 1.

Gavazzi, G. et al. 2002. *ApJ*, 576, 135.

Gilli, R. et al. 2003. *ApJ*, 592, 721.

Gioia, I. M. et al. 1999. *AJ*, 117, 2608.

Gioia, I. M. et al. 2004. *A&A*, 419, 517.

Graham, J. R. & Dey, A. 1996. *ApJ*, 471, 720.

Hammer, F. et al. 1997. *ApJ*, 481, 49.

Homeier, N. L. et al. 2004. *ApJ*, in press.

Huo, Z. et al. 2004. *AJ*, 127, 1263.

Jee, M. J. et al. 2004. *ApJ*, in press.

Joy, M. et al. 2001. *ApJL*, 551, 1.

Kinney, A. L. et al. 1996. *ApJ*, 467, 38.

Kodama, T. & Arimoto N. 1997. *A&A*, 320, 41.

Kurtz, M. J. et al. 1992. *ADASS*, 1, 432.

Longair, M. S. 1998. *Galaxy Formation*. *A&A library*. Springer-Verlag.

Lubin, L. M., Mulchaey, J. S. & Postman, M. 2004. *ApJL*, 601, 9.

Maughan, B. J. et al. 2003. *ApJ*, 587, 589.

Mercurio, A. et al. 2003a. *A&A*, 397, 431.

Moorwood, A., Cuby, J.-G. & Lidman, C. 1998. *ESO Messenger*, 91, 9.

Oke, J. B. et al. 1995. *PASP*, 107, 375.

Poggianti, B. M. et al. 1999. *ApJ*, 518, 576.

Postman, M., Lubin, L. M. & Oke, J. B. 1998. *AJ*, 116, 560.

Roettiger, K., Loken, C. & Burns, J. O. 1997. *ApJS*, 109, 307.

Romer, A. K. et al. 2000. *ApJSS*, 126, 209.

Rosati, P. et al. 1998. *ApJL*, 492, 21.

Rosati, P. et al. 1999. *AJ*, 118, 76.

Rose, J. A. 1984. *AJ*, 89, 1238.

Rose, J. A. 1985. *AJ*, 90, 1927.

Stanford, S. A. et al. 1997. *AJ*, 114, 2232.

Stanford, S. A. et al. 2001. *ApJ*, 552, 504.

Tonry, J. & Davis, M. 1979. *AJ*, 84, 1511.

Tran, K. H. et al. 1999. *ApJ*, 522, 39.

Treu, T. et al. 2003. *ApJ*, 591, 53.

van Dokkum, P. G. et al. 1999. *ApJL*, 520, 95.

van Dokkum, P. G. et al. 2000. *ApJ*, 541, 95.

van Dokkum, P. G. & Stanford, S. A. 2003. *ApJ*, 585, 78.

Wu, X., Fang, L. & Xu, W. 1998. *A&A*, 338, 813.

Xue, Y. & Wu, X. 2000. *ApJ*, 538, 65.